Design of the regenerative cooling system for a 4kN LOX/Ethanol student-built liquid rocket engine

Antoni Barredo Juan[⋆][†] *and Alberto López Platero*[⋆]
[⋆]*ISAE-SUPAERO,Université de Toulouse*
10 Avenue Edouard Belin, 31055 Toulouse, France
antoni.barredo-juan@student.isae-supaero.fr · alberto.lopez-platero@student.isae-supaero.fr
[†] Corresponding author

Abstract

PERSEUS is a European project led by students and operated by CNES, the French space agency. The aim is to allow students to engage in space related activities and gain valuable experience that will train them prior to beginning their professional activities in this sector. In this context, the Supaero Space Section technical club of ISAE SUPAERO is involved in the design of the next generation LOX/Ethanol liquid rocket engine MINERVA to be used in the sounding rocket ASTREOS 2 under development. The design of a regenerative cooling system is a building block within the vision of launcher reusability laid out by CNES as part of the evolutions of the Astreos student-built rocket. To carry out this vision, a cooling channel design and optimization tool has been developed with the objective to minimize the pressure losses while keeping the combustion wall temperature under the maximum allowable value and the coolant bulk temperature below saturation. In fact, the main technical challenge is to maintain the coolant below its critical heat flux limit, preserving its heat absorption capability. 1D heat transfer has been assumed using hot gas convection and radiation, wall conduction, and coolant convection. To account for nucleate boiling of the ethanol, a two-phase convective heat coefficient is computed along the channel and critical heat is calculated using peer reviewed correlations in the literature. Hot gas and coolant thermodynamic properties were estimated using the NASA RocketCEA and CoolProp libraries respectively. Conservation of mass, momentum and energy of the coolant was guaranteed by implementing the 1D Navier-Stokes equations. It is the objective for this tool to be used generically within PERSEUS based on chamber dimensions, propellants and target engine performance.

1. Introduction

The PERSEUS project, in collaboration with the CNES, grants aerospace engineering students the opportunity to engage in a hands-on experience in space exploration. The focus is the design of a student-built liquid rocket engine, MINERVA ($p_{cr} = 20\ bar$, $O/F = 1.4$, combustion efficiency $\eta_{c^*} = 0.8852$), to drive the ASTREOS 2 sounding rocket. A crucial part of its design is its regenerative cooling system, that should effectively regulate and manage the heat generated during combustion, to ensure optimal performance and reliability, as well as launcher reusability.

The regenerative cooling system is critical in keeping the combustion wall temperature below acceptable limits and the coolant bulk temperature below saturation, while preventing excessive pressure drop in the cooling ducts. Furthermore, the local heat transfer rate must not exceed the maximum nucleate boiling heat transfer rate at any point; instead, efforts must be made to improve coolant velocity or provide extra localized cooling, such as film cooling.

To address the technical challenges associated with the cooling system design, a specialized channel design and optimization tool has been developed. This tool incorporates correlations from peer-reviewed literature to compute the two-phase convective heat coefficient, accounting for nucleate boiling of the ethanol coolant. The regime of stable nucleate boiling is of great interest to rocket engineers as it allows for the absorption of very high heat fluxes with relatively small temperature differences between the coolant-side wall and the bulk fluid.

Additionally, this project remarks on the benefits of utilizing ethanol, as it is a suitable coolant propellant for liquid rocket engines in regenerative cooling due to its high heat capacity, low viscosity, and nucleate boiling characteristics. It absorbs a significant amount of heat before reaching its boiling point, flows easily through cooling channels, and exhibits a good nucleate boiling behaviour. Ethanol is also non-hazardous, compatible with engine materials, widely accessible, and cost-effective.

Nomenclature

Symbols

A	Area [m^2]
c_p	Constant pressure specific heat [$J/(kg \cdot K)$]
D	Diameter [m]
G	Mass flow rate [$kg/m^2/s$]
h	Heat flux coefficient [$W/(m^2 \cdot K)$]
H	Enthalpy [J/kg]
$\tilde{h}$	Height [m]
L	Longitude [m]
L_{lv}	Latent heat of vaporization [J/kg]
M	Mach number
Nu	Nusselt number
O/F	Mixture ratio
p	Pressure [Pa]
Pr	Prandtl number
q	Heat flux [W/m^2]
Re	Reynolds number
T	Temperature [K]
t	Thickness [m]
V	Velocity [m/s]
x	Vapor quality

Greek letters

γ	Specific heat ratio
κ	Thermal conductivity [$W/(m \cdot K)$]
ρ	Density [kg/m^3]
σ	Surface tension [N/m]
μ	Viscosity [$Pa \cdot s$]

Subscripts

c	Coolant
ch	Channel
cr	Chamber
fc	Forced convection
fb	Forced convection and nucleate boiling
g	Hot gases
l	Liquid phase; fluid
mw	Mid-wall
nb	Nucleate boiling
sat	Saturation state
sub	Subcooled
t	Throat
v	Vapor
w	Inner wall
0	Total

2. Modelling approach

A first-order steady-state model has been developed. These methods are fast and allow researchers to analyze many design factors. Nevertheless, due to semi-empirical correlations, its accuracy is frequently poor. The first-order approach determines thermal equilibrium in different sections of the nozzle and combustion chamber. As a first iteration, the model includes convection and radiation from the hot gas to the wall, conductivity through the wall, convection from the wall to the coolant flow, and the fin effect on coolant convection. Longitudinal and circumferential heat transfer are neglected. Therefore, the previous statements lead us to

$$q = h_g \left(T_{aw} - T_{w,g}\right) + q_{rad} = \frac{\kappa_w}{t_w}\left(T_{w,g} - T_{w,c}\right) = h_c \left(T_{w,c} - T_c\right) \tag{1}$$

where T_{aw} is the adiabatic wall temperature and q_{rad} is the heat flux due to radiation of the hot gases.

2.1 Hot gas side

The heat exchange between the hot gases and the walls is dominated by the thermal and viscous boundary layer. The adiabatic wall temperature T_{aw} is the temperature the flow would reach in contact with the wall in case the heat flux is equal to zero. In a laminar flow with a Prandtl number equal to unity, this temperature would match the stagnation temperature of the flow. In other flow case and turbulent fluid, the adiabatic wall temperature differs from the stagnation temperature and it can be estimated by using different recovery factors which depend on the Prandtl number. For turbulent boundary layers,[2] $r = Pr^{1/3}$.

$$T_{aw} = T_g \left(1 + r\frac{\gamma - 1}{2}M^2\right) \tag{2}$$

2.1.1 Convective heat transfer

Regarding the convective heat transfer coefficient, the Bartz equation is the most well known formulation. A detailed analysis of the flow at the boundary layer can led to the following relation

$$Nu = Re^m Pr^n f(\sigma) \tag{3}$$

where m, n are coefficients that are set empirically and depend on the type and flow configuration. The σ represents the temperature variation, in such a way that $f(\sigma)$ takes into account the variation of the fluid transport properties

along the boundary layer. For liquid rocket engine applications where the flow is turbulent, it is usual to take $m = 0.8$ and $n = 0.4$, and Bartz proposed[2] $f(\sigma) = 0.026$.

Inside the nozzle, due to the longitudinal pressure gradient, the boundary layer at the wall is accelerated. Therefore, the thickness of the boundary layer is constrained, modifying its convection heat transfer rate. Considering the previous statements, Bartz takes Eq. 3 and introduces the effects of pressure gradient along the nozzle, as well as the variation of properties with the temperature through the boundary layer, leading to the following expression

$$h_g = C\{\mu^{0.2} c_p Pr^{-0.6}\}_{g0} p_{cr}^{0.8} (c^*)^{-0.8} D_t^{-0.2} (A/A_t)^{-0.9} \delta \tag{4}$$

where c^* is the characteristic velocity and $\{\ \}_{g0}$ means evaluated at the stagnation temperature T_{g0}, which in the most simple case can be approximated as the chamber temperature $T_{g0} \sim T_{cr}$ (i.e. composition outside the boundary layer). Moreover, the factor δ can be expressed as

$$\delta = \left[\frac{1}{2}\frac{T_{w,h}}{T_{cr}}\left(1 + \frac{\gamma - 1}{2}M^2\right) + \frac{1}{2}\right]^{-0.68}\left(1 + \frac{\gamma - 1}{2}M^2\right)^{-0.12} \tag{5}$$

Observing Eq. 4, as the heat flux scale with $D_t^{-0.2}$, small nozzle will require extract more heat per unit of area. Moreover, as the heat flux scale with $p_{cr}^{0.8}$, for engine with high chamber pressures, the heat flux will be relatively higher. The most notable influence is due to the last term $(A/A_t)^{-0.9}$ which, in addition to the boundary layer thickness diminution, manifests that the heat flux will be maximum at the nozzle throat. Furthermore, the δ factor diminishes with the increase of the Mach number. Therefore, for equal area relation, the supersonic section will be less demanded than the subsonic section. It should be noted that the value of the constant $C = 0.026$ was determined for a specific rocket nozzle and may need to be adjusted to better match numerical or experimental data if it becomes available.

2.1.2 Radiative heat transfer

In addition to considering convective heat transfer, the model also incorporates the impact of radiative heat transfer from the hot gases to the wall. This aspect is particularly significant for small rocket engines. The presented method was studied for small RP-1 and gaseous oxygen rocket engines. Given that the main gases in a rocket chamber are H_2O, CO_2, and CO, a model for the first two is provided since it is estimated that the radiation provided by carbon monoxide is an order of magnitude lower than carbon dioxide[16]

$$q_{rad,H_2O} = 5.74 \cdot (P_{H_2O} \cdot r_s)^{0.3} \cdot \left(\frac{T_{aw}}{100}\right)^{3.5} \tag{6}$$

$$q_{rad,CO_2} = 4 \cdot (P_{CO_2} \cdot r_s)^{0.3} \cdot \left(\frac{T_{aw}}{100}\right)^{3.5} \tag{7}$$

where p_{CO_2} and p_{H_2O} are the corresponding partial pressures and r_s is the radius of the engine section. It is worth noting that the current model does not present a temperature to the power of four, which is how radiative heat transfer actually varies with temperature. As a result, at lower temperatures, the radiative heat transfer will likely be underestimated.

2.2 Coolant flow

The coolant flow is modeled using steady-state principles of mass, momentum and energy, taking into account heat transfer and friction effects. It is simplified to a one-dimensional representation, where the velocity and flow variables vary solely with distance along the x-axis. The shear stress is determined by the flow variables and a skin friction factor f, while the heat flux is only due to convection. To describe the skin friction factor f and the heat transfer coefficient h_c, semi-empirical correlations are employed in consideration of the aforementioned set of equations.

The model accounts for variations in coolant velocity as it flows through the channels, which results in changes in static pressure and static temperature. As a result, the temperature for a new section is determined by adding the preceding step's temperature plus the temperature change due to the heat transfer and the difference between the kinematic terms. The pressure drop between sections is mostly due to the viscous effect, which can be evaluated using Darcy's law,

$$\Delta p = \frac{f\rho V^2 \Delta L}{2D_h} \tag{8}$$

where ΔL is the longitude between sections of the channel and D_h the hydraulic diameter of the channel. The skin friction factor f is evaluated by following Colebrook's semiempirical relation[18]

REGENERATIVE COOLING LIQUID ROCKET LOX/ETHANOL

$$\frac{1}{\sqrt{f}} = -2\log\left(\frac{0.27e}{D_h} + \frac{2.51}{Re\sqrt{f}}\right) \tag{9}$$

The assumption of constant fluid characteristics is used in this analysis, which is only suitable for adiabatic walls and moderate velocities. Fluid properties, mainly temperature-dependent, vary across the flow cross-section of a tube and are complicated by different fluid behaviors. For liquids, specific heat and thermal conductivity are relatively constant with temperature, but parameters like the viscosity or the Prandtl number vary with temperature.

2.2.1 Heat transfer coefficient

The operation of rocket engines under unusual conditions, such as high heat flux rates and certain coolant states, has shown unexpected phenomena. Understanding these processes is critical for maximizing coolant heat transfer in liquid propellant rocket engines. The purpose of this part is to provide a qualitative overview of forced convection processes at high heat fluxes, as well as to present appropriate numerical prediction methodologies for analyzing the influence of various phenomena on coolant heat transfer.

When the coolant remains in the liquid phase throughout the duct, heat transfer occurs through single-phase forced-flow convection. The heat flux from the heated surface to the coolant is directly proportional to the temperature difference between the coolant-side wall and the bulk fluid

$$q_{fc} = h_{fc}(T_{w,c} - T_c) \tag{10}$$

High-intensity heat transfer in forced flow convection systems is often studied using simplified versions of the Nusselt equation. Reference temperatures and dimensionless functions are introduced to account for specific effects, such as the temperature difference between the wall and the fluid. The well-known Sieder-Tate equation incorporates a viscosity ratio function[7]

$$h_{fc} = 0.027 Re_l^{0.8} Pr_l^{0.4}\left(\frac{\mu_l}{\mu_w}\right)^{0.14}\frac{k_l}{D_h} = Nu_{fc}^0\frac{k_l}{D_h} \tag{11}$$

where all physical properties are evaluated at the bulk temperature, except for the viscosity at the coolant-side wall temperature. The Nu_{fc}^0 is the forced convection Nusselt number without curvature and roughness correction. This equation is reasonably accurate for $0.7 < Pr < 16700$, $Re > 10^4$ and $L/D > 10$.

As heat flux increases, the temperature difference between the wall and the liquid rises until the wall temperature reaches the boiling point of the coolant. At this point, vapor bubbles form on the heated surface and immediately condense upon detachment due to the lower coolant temperature. Higher heat flux causes more frequent bubble formation and collapse, disrupting the laminar sub-layer and increasing heat transfer rates compared to single-phase convection. This regime starts when the surface temperature is slightly above the saturation temperature of the coolant, known as the onset of nucleate boiling (ONB). As more nucleation sites are activated beyond ONB, the wall temperature begins to level off. Different approaches are presented in the literature to define a nucleation criterion. One of the methods introduced an equation to compute the difference in temperatures between the wall and the saturation temperature of the fluid[15]

$$\Delta T_{sat,ONB} = \frac{4\sigma T_{sat}v_{lv}h_{sp}}{k_l L_{lv}}\left(1 + \sqrt{1 + \frac{k_l L_{lv}\Delta T_{sub}}{2\sigma T_{sat}v_{lv}h_{sp}}}\right) \tag{12}$$

where h_{sp} is the heat transfer coefficient for single-phase flow and v_{lv} the latent specific volume.

The correlation of Chen[6] is a superposition model that combines nucleate pool boiling with forced convection. Chen's model can be generalized in the following correlation for calculating the total heat

$$q_{fb} = F \cdot q_{fc} + S \cdot q_{nb} \tag{13}$$

The q_{fc} single-phase convective heat flux can be obtained from Eqs. 10-11, and q_{nb} can be estimated using pool boiling predicting correlations proposed by Forster and Zuber[11]

$$h_{nb} = 0.00122\frac{k_l^{0.79}c_{p,l}^{0.45}\rho_l^{0.49}g^{0.25}}{\sigma^{0.5}L_{lv}^{0.24}\rho_v^{0.24}\mu_l^{0.25}}\Delta T^{0.24}\Delta p^{0.75} \tag{14}$$

where g is the gravity constant. In Eq. 13, the correlation for forced convection is the temperature difference between the heating wall and the fluid, and the nucleate boiling relation is the temperature difference between the wall and the saturated temperature of the fluid. Therefore, it can be converted into an equivalent heat transfer coefficient as

$$h_{fb} = F \cdot h_{fc} + S \cdot \frac{T_w - T_{sat}}{T_w - T_c} h_{nb} \tag{15}$$

The dimensionless function F is an enhancement factor indicating the micro-convection which happens due to the liquid cavity formation and restoration when bubbles form and depart the heating surface. It is defined as

$$F = \left(\frac{Re_{tp}}{Re_l}\right)^{0.8} \tag{16}$$

where Re_{tp} is the two-phase Reynolds number. According to the previous expression, F is close to unity in subcooled flow boiling, which is equal to not considering the interference of bubbles from the heating surface. This assumption is valid for light boiling but not for intense boiling in low-velocity conditions. For the assessment of the convective heat transfer enhancement factor F and the nucleate boiling suppression factor S, the author originally provided two graphical functions. The more precise expression[8] of enhancement factor F is a function of Martinelli parameter X_{tt}, as proposed by Chen[6]

$$F = \begin{cases} 1 & if\ 1/X_{tt} \le 0.1 \\ 2.35\,(1/X_{tt} + 0.213)^{0.736} & if\ 1/X_{tt} > 0.1 \end{cases} \tag{17}$$

where the Martinelli parameter X_{tt} evaluates the boiling intensity

$$X_{tt} = \left(\frac{1-x}{x}\right)^{0.9} \left(\frac{\rho_v}{\rho_l}\right)^{0.5} \left(\frac{\mu_l}{\mu_v}\right)^{0.1} \tag{18}$$

The local vapor mass fraction x can be derived from a widely used correlation proposed by Kandlikar[15]

$$x = -c_{p,l} \frac{(T_{sat} - T_c)}{L_{lv}} \tag{19}$$

The dimensionless function suppression factor S originally proposed by Chen is based on the relation of the effective superheat. Therefore, it is possible to find in the literature different correlations for the suppression factor. Among them, one of the best-fitting analytical expressions is[8]

$$S = \frac{1}{1 + 2.53 \times 10^{-6}(Re_l F^{1.25})^{1.17}} \tag{20}$$

In order to quantify the geometry and chamber material, a correction factor is applied on heat transfer, particularly important since the additive manufactured engine has greater roughness compared to conventionally machined parts. An expression is derived for the roughness correction factor[18]

$$C_\xi = \frac{1 + 1.5Pr^{-1/6}Re^{-1/8}(Pr - 1)}{1 + 1.5Pr^{-1/6}Re^{-1/8}(Pr\xi - 1)} \xi \tag{21}$$

where $\xi = f(Re, \varepsilon)/f(Re, \varepsilon = 0)$ is the ratio of the rough tube isothermal friction factor to the smooth one. Moreover, a curvature correction factor is introduced to account for secondary flow effect induced in a curved channel

$$C_I = \left[Re\left(\frac{D_h}{2R}\right)^2\right]^{\pm 0.02} \left[1 + 0.32 \sin\left(\pi \sqrt{\frac{s}{L + 15D_h}}\right)\right] \tag{22}$$

where s is the curvilinear coordinate and L is the total longitude of the curve. The impact of roughness and curvature is modeled by including these factors in the forced convection Nusselt number

$$Nu_{fc} = Nu_{fc}^0 \cdot C_\xi \cdot C_I \tag{23}$$

In case of taking into account the presence of the ribs, the coefficient must be corrected. The fin efficiency η_f can be defined as[21]

$$\eta_f = tanh\left(\left(\frac{2 \cdot h_c t_{mw}}{k_c}\right)^{0.5} \frac{\tilde{h}_{ch}}{t_{mw}}\right)\left(\left(\frac{2 \cdot h_c t_{mw}}{k_c}\right)^{0.5} \frac{\tilde{h}_{ch}}{t_{mw}}\right)^{-1} \tag{24}$$

which modifies the convective heat transfer coefficient

$$h_{c,f} = h_c \frac{w_{ch} + 2 \cdot \eta_f \cdot \tilde{h}_{ch}}{w_{ch} + t_{mw}} \tag{25}$$

It is worth mentioning that the effect of having a rectangular non-uniformly heated channel on the correlation has not been examined. Seeing as how there is a scarcity of experimental evidence on ethanol working in these extreme conditions, it was found suitable to use a more conservative model in this regard.

2.2.2 Critical Heat Flux (CHF)

With further increases in heat flux, the Departure from Nucleate Boiling (DNB) may occur. The heated surface experiences the formation of vapor pockets as the heat flux rises. Eventually, a maximum heat flux is reached, which causes the individual bubbles to merge, generating a continuous layer of vapor. At this stage, the temperature gradient across the boundary layer is primarily influenced by the presence of the vapor film rather than the liquid coolant. Due to the significantly lower thermal conductivity of the vapor film compared to the liquid phase, a considerably larger temperature difference is necessary to maintain a heat flux slightly above the DNB point. Consequently, DNB poses a potential threat to both the operational safety and the lifespan of the engine.

In order to avoid or delay the DNB, it is necessary to predict accurately the CHF in subcooled flow boiling at high pressure and high heat flux. The available experimental data is limited for subcooled flow boiling (mainly for water). In the open literature, various CHF correlations for subcooled water flow boiling have been mentioned. However, for high heat flux and high pressure, the accuracies of the CHF correlations for predicting subcooled flow boiling may be inadequate. Among all the correlations found in the literature, the modification of the Tong correlation was chosen since it best fits the experimental data.[5] Furthermore, its margin of validation covers the range of operation of the system [$2200 < G < 4 \times 10^4 kg/m^2/s$; $1 < p < 50 bar$; $2.5 < D < 8mm$; $12 < L/D < 40$; $15 < \Delta T_{sub} < 190K$; $4 < q_{CHF} < 60MW/m^2$]

$$q_{CHF} = C \frac{L_{lv}G}{Re^{0.5}} \quad ; \quad C = \psi(0.216 + 4.74 \times 10^{-2}p) \tag{26}$$

$$\psi = \begin{cases} 0.825 + 0.986x & if \; -0.1 < x < 0.1 \\ 1 & if \; x \leq -0.1 \\ 1/(2 + 30x) & if \; x \geq 0 \end{cases} \tag{27}$$

2.3 Film cooling

The behaviour between the heat flux and the CHF in the nozzle and combustion chamber, clearly shows that the heat transfer requirements exceed the cooling capacity of the regenerative cooling system alone, potentially leading to local hot spots and overheating of the cooling channels. Moreover, due to the limitations imposed by the geometry tolerance, it is not feasible to raise the coolant velocity sufficiently to achieve the desired increase in Critical Heat Flux (CHF). Consequently, to address this issue, a film cooling system is introduced as a supplement to the existing regenerative cooling system.

The mechanisms involved in liquid film are depicted in Fig. 1. Heat is transferred from the hot gases to the liquid film by convection. The energy is absorbed in heating up the film on the wall until the saturation temperature. The vapor generated flows outward from the liquid film, decreasing the normally expected convective heat flux. Downstream of the liquid film, the vapor mixes with the free stream gas entrained in the boundary layer, lowering the wall temperature through gaseous film cooling.
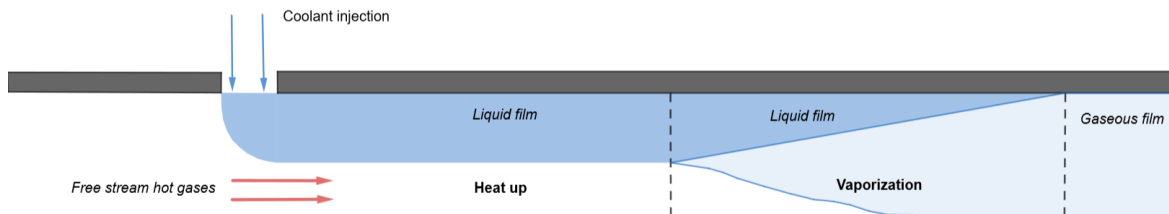

Figure 1: Film cooling mechanism

2.3.1 Liquid film cooling formulation

For the liquid film formulation, it has been used the well know correlation of Grisson to estimate the local heat transfer coefficient.[12] Only convection heat transfer has been taken into account. The mentioned reference provides a heat

transfer coefficient for the heat up segment as well as an alternative heat transfer coefficient once the liquid reaches the saturation temperature h_{film}.

The heat flux absorbed by the film is described in Eq. 28. The energy transferred to the film will provoke a temperature rise as defined in Eq. 29.

$$\dot{q}_{film} = h_{film}(T_g - T_l) \tag{28}$$

$$\frac{dT_l}{dx} = 2\pi r_{nozzle} \frac{\dot{q}_{film}}{\dot{m}_{film}c_{p,l}} \tag{29}$$

Once the saturation temperature is reached, the convective heat flux with transpiration is calculated implicitly which will be slightly lower than the previous segment transfer coefficient. The heat flux absorbed by the film is computed using the same expression as in Eq. 28. Finally, the liquid evaporates at a rate,

$$\dot{m}_{vap} = \frac{\dot{q}_{film}}{L_{lv}} \tag{30}$$

2.3.2 Gaseous film cooling formulation

After the liquid has vaporized, it continues to provide thermal protection to the wall by calorimetric mixing with the hot free stream gas entrained in the boundary layer. Numerous formulations have been presented for this process. In this study, it has been used the NASA Appendix B model.[1] The existence of gaseous film cooling will vary the adiabatic wall temperature, and thus, the total heat flux

$$T_{aw} = \frac{H_{aw} - \eta H_{c,v} + \eta c_{p_v} T_{if} + (1 - \eta)(c_{p_g} T_{0,g} - h_g)}{\eta c_{p_v} + (1 - \eta)c_{p_g}} \tag{31}$$

where H_{aw} is the adiabatic wall enthalpy, and T_{if} is the saturation temperature corresponding to the partial pressure of the vapor. The film cooling efficiency η can be obtained from

$$\eta = \frac{1}{\theta(1 + W_E/W_c)} \tag{32}$$

where W_E/W_c is the entrainment flow ratio and θ is the shape factor for the mixing-layer profile, which can be obtained from empirical correlations.[1]

2.4 System

The system has been implemented in Python. The program initiates by injecting coolant through the nozzle exit where the initial measurement station is located, which then flows towards the injector. Once a steady state is achieved for the heat flux at this location, the program proceeds to the subsequent measurement station. The inputs of the program consist mainly of the engine material and geometry, along with combustion parameters. The hot gas values are obtained using the software Chemical Equilibrium with Applications (CEA) developed by NASA, while the coolant properties are computed using CoolProp library.[3] The system variables are the number of channels, the width, the hot wall thickness, and the aspect ratio. The outputs of the program are the wall temperature, the heat flux, and the evolution of the coolant along the channel. The structure of the model is based on reading the parameters, computing the coolant state, and iteratively seeking convergence of the wall temperature. Once the wall temperature is converged, the program passes to the next station until reaching the final station.

Among the assumptions taken into account, only radial heat transfer is considered, and no deformation of the wall. Also, the hot gases are computed considering chemical equilibrium until the throat, where the gas composition is frozen. Finally, the coolant properties are considered uniform and constant in each section.

3. Validation

3.1 System

In an ideal scenario, the developed model would be validated by comparing it with experimental data acquired from a rocket engine that, in terms of propellants, thrust level, and *OF* ratio, closely correspond to the reference engine. This validation approach would entail analyzing the accuracy of the one-dimensional model as well as calibrating the Bartz

equation, an empirical equation that varies depending on the engine. Unfortunately, no relevant engine or test data pertaining to the LOX/Ethanol engine used in this paper could be found in the current literature.

As a consequence, the model is instead compared to CFD results from a LOX/Methane engine experiment carried out by the Italian Aerospace Research Center (CIRA).[20] This comparison is intended to confirm the heat transmission processes within the engine's wall. Nevertheless, because a large part of the flow was at supercritical temperatures, Taylor's correlation was used for the Nusselt calculation.[22] As a result, the coolant side heat transfer coefficient cannot be entirely confirmed, serving this validation as a validation of the code's system.

A conjugated heat transfer analysis using an axisymmetric 2D CFD for the combustion gases is used as the reference simulation. The combustion products were expected to be completely burned when they entered the chamber and then frozen in composition. A 3D RANS simulation is used for the cooling channels. Curvature correction was not accounted for, as geometrical parameters of the nozzle were not available. No radiation heat transfer is modeled. The coolant enters the chamber at the end of the nozzle and then flows towards the injector. The combustion chamber conditions are an engine pressure of 56 bar and a mixture ratio of 3.35. A flow rate of 20 g/s was specified across each of the 96 cooling channels was specified, with an inlet pressure of 155 bar and an inlet temperature of 110 K.

(a) Hot gas side heat flux coefficient

(b) Heat flux

(c) Hot gas side wall temperature

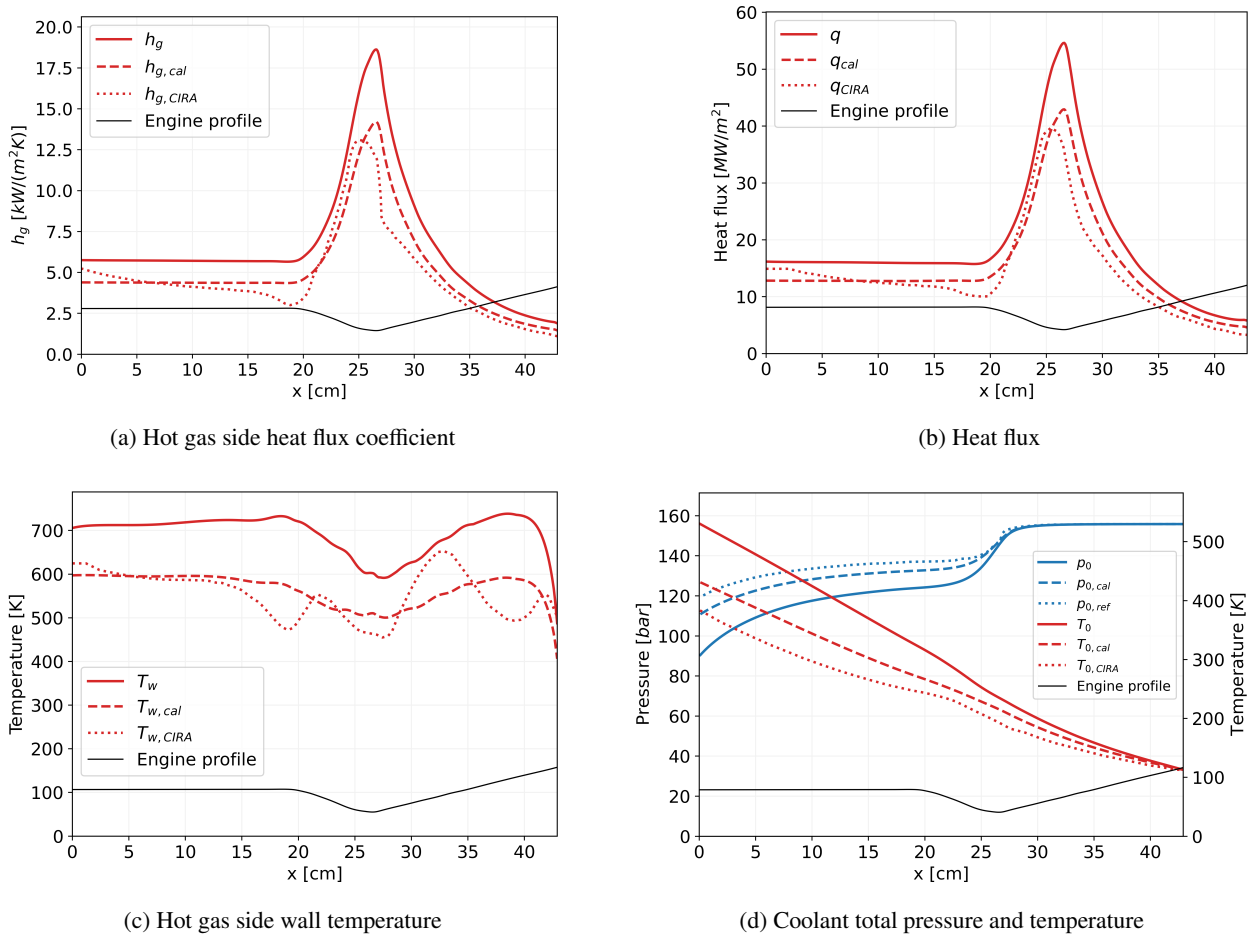(d) Coolant total pressure and temperature

Figure 2: Comparison of calculated, calibrated, and CIRA reference values along the engine.

The comparison of the model with the CFD results is presented in Figure 2. Firstly, it can be observed in Fig. 2a that the current model overpredicts a 42% of the maximum heat flux coefficient. The Bartz equation may overestimate the heat transfer coefficient. According to a recent study,[16] the empirical constant of the Bartz equation can be reduced by up to 25% for this engine. It is important to note that the ideal case would be to gather experimental data for the studied engine (in this case, LOX/Ethanol) to fit the correlation. Furthermore, in contrast to the CFD simulation, the results obtained with Bartz's correlation remain constant at the cylindrical section. This is because Bartz's equation is based on the local area ratio and does not take into account the development of the boundary layer, hence, its increasing thickness.[4] Nevertheless, it can be deduced that the 1D model, when compared to the more thorough 3D CFD analysis, shows comparable tendencies in the outcome attributes. This suggests that the model is capable of generating results that are valuable for preliminary analyses.

In the case of the heat flux, Fig. 2b illustrates an overprediction of 37.6% compared to the reference value. Once the Bartz equation is tuned, the relative error diminishes up to 8%. In Fig. 2c the predicted values of the wall temperature result far from the reference value, averaging approximately 100K. Furthermore, the contour of the wall temperature along the nozzle differs notably. Both studies reveal a clear temperature minimum near the throat. The reference analysis also has two local minima on either side, which were attributed to the cooling channel geometry of this specific engine.

Finally, the evaluation of the thermodynamic state of the coolant flowing through the channels can be observed in Fig. 2d. The coolant is flowing in the opposite direction of the combustion gases. It starts with high pressure and low temperature, heating up and losing pressure while moving towards the combustion chamber. The trends of both curves are very similar. Because of the low coolant velocity and heat flux, the total coolant pressure remains virtually constant at the diverging region of the nozzle. At the region near the throat, there is a steep drop in total pressure associated with the maximum heat flux and the narrowing of the cooling channels. After this abrupt decrease, the pressure curve levels off, but its slope gradually increases again at the end of the channel. This increase is due to the narrowing of the cooling channel. Although the trend is very similar, the absolute value of the pressure drop is 65.35 *bar*, for the calibrated model a pressure drop of 45 *bar*, as opposed to 35.6 *bar* for the coupled 3D analysis. When analyzing the temperature profiles of the coolant, the trends show again a considerable similarity once again. The temperature increases relatively constant, with a small steepness near the location of maximum heat flux. The total temperature increase is 417 *K*, for the calibrated 318 *K*, while the reference analysis predicts only an increase of 271 *K*.

Nevertheless, since the performance of this reference engine does not correspond to the case of this study, no substantial error results should be taken, instead, what should be appreciated is the capability of the system to predict qualitatively the behaviour of the cooling system. As for the coolant heat transfer correlation for ethanol, the concept of superposition calculation is widely accepted. Many variations of the Chen's model have been made through the years (i.e. Gungor-Winterton[13]). These correlations have been tested and compared against experimental data for ethanol[19] in its saturated state within a heat flux range of 10-40 kW/m^2. However, it is important to note that rocket engines operate under much higher heat flux conditions, reaching the megawatts range. Due to the significant difference in heat flux levels, there is currently no experimental data for ethanol available to validate the existing correlations for such extreme conditions.

In order to search for a correlation that could better fit the conditions of the system, correlations like Gungor-Winterton adopted the formula for pool boiling proposed by Cooper.[9] Nevertheless, it has been observed a significant deviation of experimental data and the prediction result of Cooper's correlation at high heat fluxes ($250 MW/m^2$) for the refrigerant R134a.[14] Moreover, despite the effort made to adapt Chen's model for subcooled boiling flow,[7] to show how the enhancement factor increases with the velocity, since the validation has been made for a range of low values of heat flux, it has been followed the assumption of Gungor-Winterton, that defined an enhancement factor F equal to unity for subcooled boiling flows. Nevertheless, it is necessary to mention that this assumption is controversial since bubbles still occur in subcooled boiling flows.

Finally, an extensive study was carried out for subcooled water at high heat fluxes[17] (MW/m^2). It was found that the Chen correlation was one of those which better fitted the experimental data, applying the respective adaptations for subcooled flow boiling. Therefore, the modified Chen's correlation is used in this study.

4. Results

4.1 Multi-objective optimization using Genetic Algorithm

The optimization is aimed to define the geometry of the channels along the engine, given an inlet pressure of 30 *bar* and an inlet temperature of 300 *K*. It will be focus on reducing the impact of the most restrictive variables, the temperature of the wall, the saturation margin of the coolant and the critical heat flux. Firstly, the maximum wall temperature at the throat should be lower than 1260 K, respecting a 25% security margin for Inconel 718 melting point. Secondly, the requirement for a larger saturation margin of the coolant has been imposed in order to avoid the formation of vapor droplets, allowing the fluid to arrive at the expected conditions at the injector. The last objective function is imposed due to the fact that if the heat flux exceeds the CHF, the formation of a stable liquid-vapor interface becomes challenging, leading to an accumulation of vapor and a reduction in heat transfer efficiency. In a normal circumstance, the CHF problem would be included in constraints. However since it is unfeasible that this constraint can be fulfilled without deeply degrading the pressure drop, it has been added to the set of cost functions in order to minimize its impact. The optimization problem can be defined as,

REGENERATIVE COOLING LIQUID ROCKET LOX/ETHANOL

$$\begin{cases} f_1 = min(Wall\ temperature|_{throat}(\mathbf{x})) \\ f_2 = max(Saturation\ margin|_{init\ CC}(\mathbf{x})) \quad s.t. \begin{cases} g_1 = t_{mw}(\mathbf{x}) \geq 1\ mm \\ g_2 = \tilde{h}_{ch}(\mathbf{x}) \geq 0.7\ mm \end{cases} \quad \mathbf{x} = \begin{pmatrix} AR \\ N_{ch} \\ t_{hot\ wall} \\ t_{mw} \end{pmatrix} \quad (33) \\ f_3 = max(CHF(\mathbf{x}) - q(\mathbf{x})) \end{cases}$$

It is imperative to carry out a sensibility study in order to analyze the impact of each variable, given the multi-objective cost function and the multiple optimization variables. Fig. 3 shows that the hot wall thickness follows a tendency that simultaneously optimizes each objective function. Thus, hot wall thickness is desired to be minimized to its lowest extent (1 mm). Nevertheless, although the mid-wall thickness has a minor relevance in the maximum temperature, it cannot meet one objective function without adversely affecting the other. The three remaining variables are interrelated.
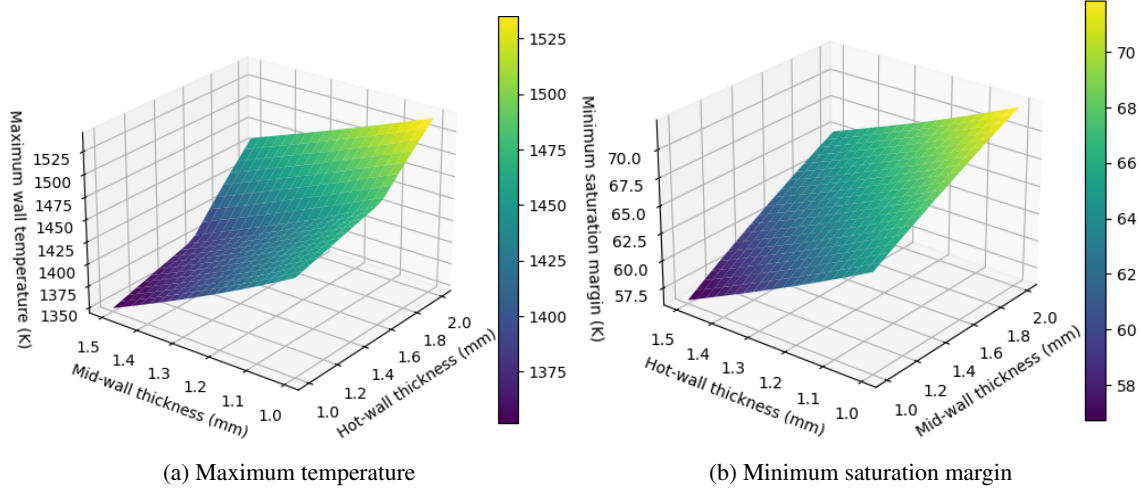

(a) Maximum temperature

(b) Minimum saturation margin

Figure 3: Hot wall and mid wall thickness influence, N_{ch} = 57, AR = 6.

Following the definition in Eq. 34, both the number of channels and the mid-wall thickness contribute to the width value. Due to geometrical restrictions, the number of channels N_{ch} will remain fixed at a value of 57 channels. Finally, the optimization variables will be w_{ch} and AR. The reason why w_{ch} has been chosen instead of t_{mw} lies on its direct consequence in coolant velocity without taking into account the radius.

$$w_{ch} = \frac{2\pi r_{nozzle}}{N_{ch}} - t_{mw} \qquad \tilde{h}_{ch} = AR\, w_{ch} \qquad (34)$$

As shown in the left Fig. 4, three regions are considered along the engine. For most rocket systems, the throat region is the most critical part regarding higher heat flux, wall temperature and CHF. Meanwhile, the minimum saturation margin is reached at the beginning of the combustion chamber.
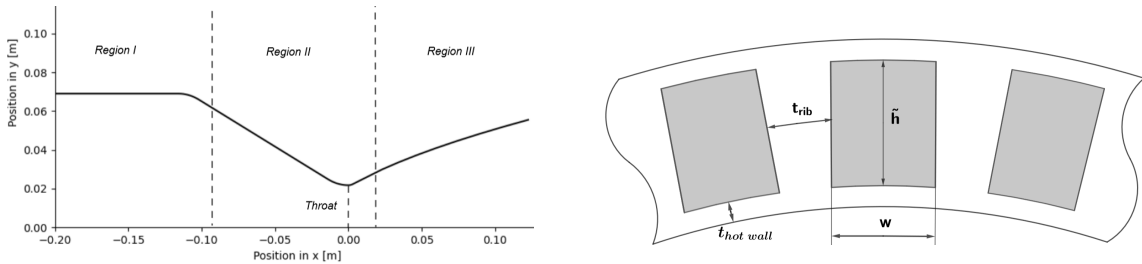

Figure 4: Nozzle trace and channel geometry

Given this configuration, the design criteria applied to regions II and III will prioritize a lower wall temperature while a greater saturation margin criteria will be applied for the region I.

In an ideal scenario, the CHF would never be exceeded throughout the whole system, but this condition would translate into both a strong pressure drop and a decrease in the saturation temperature margin. In case of working only with regenerative cooling the CHF condition will be highly prioritized in region II. Nevertheless, it has been suggested

to include film cooling, which conveniently decreases the heat flux, specially in the vicinity of the throat. The addition of film cooling therefore enables the possibility of optimizing the geometry in a way that the heat flux always stays below the CHF in regions I and III, by rising it. This way, the coupling of regenerative and film cooling enables a compromise for which the heat flux never surpasses the CHF.
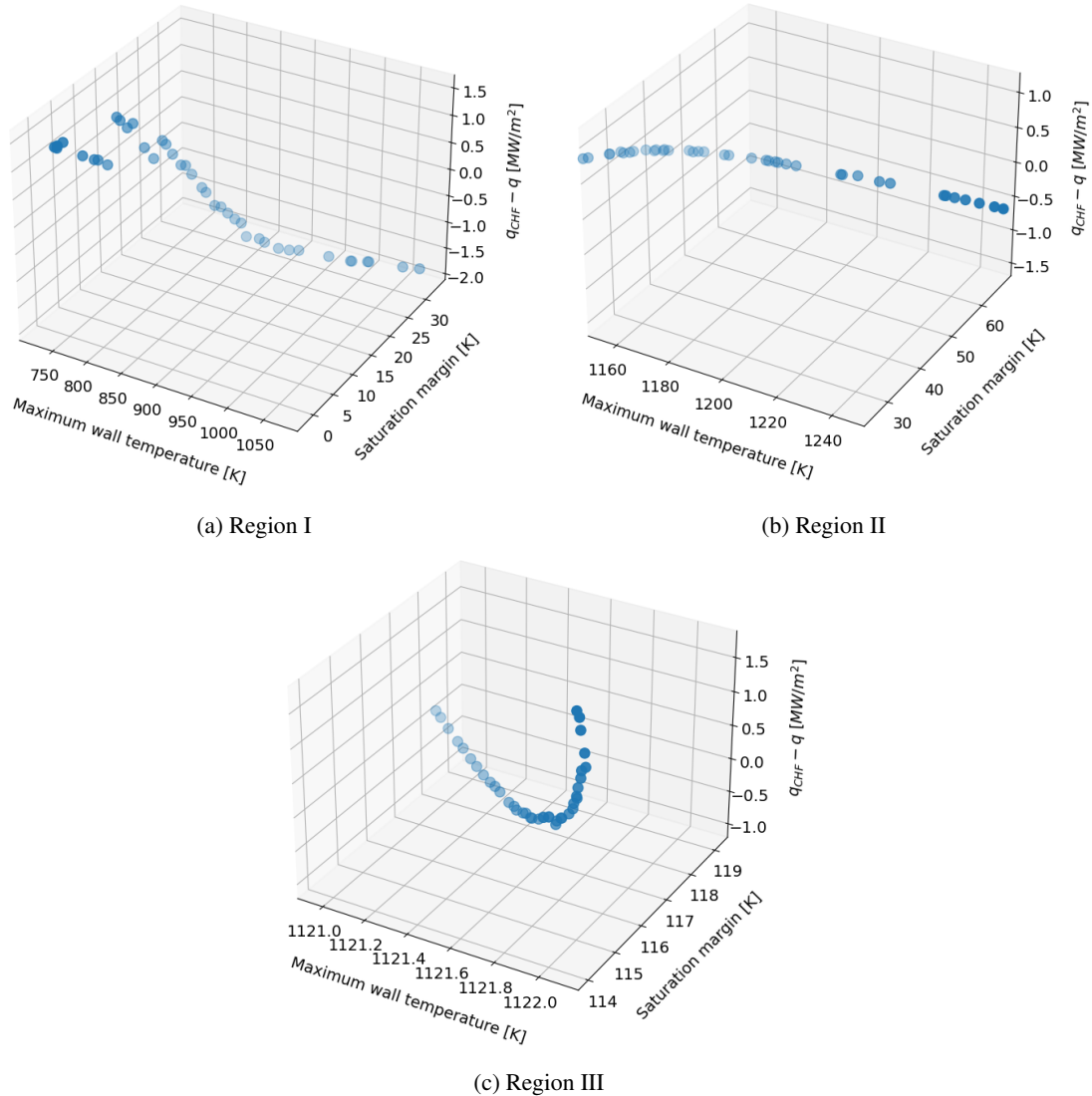

(a) Region I

(b) Region II

(c) Region III

Figure 5: Pareto fronts

The optimization concept that has been adopted is a Genetic Algorithm (GA) inspired by the process of natural selection and genetic combination. In nature, weak and unfit species within their environment are faced with extinction and the strong ones have a greater opportunity to pass their genes to future generations. The reason why this computational approach has been embraced lies in its suitability for optimizing black box functions where explicit mathematical formulations or gradients are unavailable, and in its efficient constraint handling. Furthermore, GA can effectively generate a Pareto front, providing a set of trade-off solutions that represent different compromises between objectives.

The optimization algorithm utilized is an elitist non-dominated genetic algorithm, NSGA-II.[10] Given the optimization variables w_{ch} and AR, none of the objective functions can be improved without degrading some of the other objective values, what is called non-dominated solution. Moreover, elitism ensures that the best solutions found so far are not lost during the evolutionary process, preserving the Pareto front and preventing premature convergence.

Given the Pareto front obtained for each segment in Fig 5, the following restrictions have been applied in order to search for the desired design space. For region I, $T_{max} < 1175K$, $\Delta T_{sub} > 30K$, $min(q_{CHF} - q) > 0$; for region II, $T_{max} < 1200K$; and for region III $T_{max} < 1000K$, $min(q_{CHF} - q) > 0$. It is worth noting that in Fig 5c the maximum

REGENERATIVE COOLING LIQUID ROCKET LOX/ETHANOL

wall temperature presents a faint variation because the maximum temperature will be always reached in the frontier between region II and III. Thus, changes in region III channels while maintaining a constant geometry for region II will result in a low variation in maximum hot wall temperature.
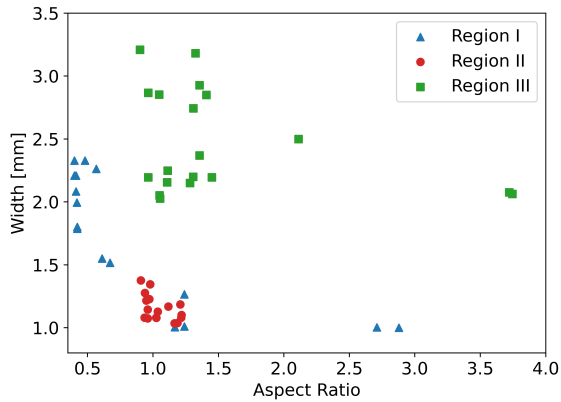

Figure 6: Design space selected

Table 1: Final geometry of regions/critical points

	Region I Chamber	Region II Throat	Region III Average
AR	0.6	1.1	1.2
w_{ch}	2.2	1.2	2.7

Fig 6 illustrates a feasible geometry able to meet the previous requirements. Nevertheless, some geometry combinations could lead to undesired values for ΔT_{sub}, given that the optimization of each region have been carried out using a constant geometry for the rest of segments. Regardless of the channels geometry from segment I, if the velocity in segments II and III is high, ΔT_{sub} at the beginning of segment will be severely affected. This issue does not apply to CHF and maximum wall temperature. There are two clear zones for regions I and II, while for region III different

(a) Heat flux

(b) Hot and cold wall temperatures

(c) Channel geometry
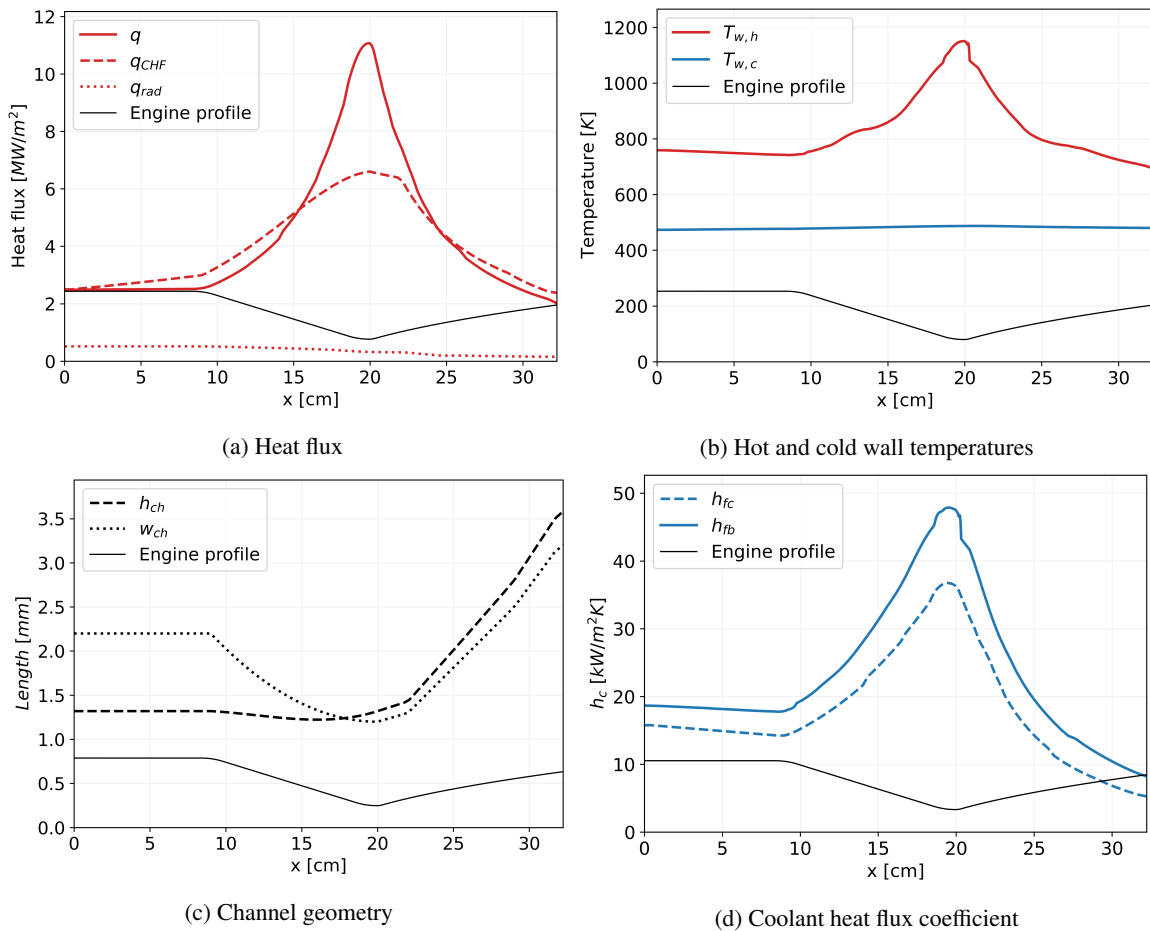

(d) Coolant heat flux coefficient

Figure 7: Results obtained with regenerative cooling along the engine axis

configurations are possible. The channel geometry has been defined by selecting the optimal dimensions for the regions/critical points (Tab. 1), using a quadratic interpolation between regions I and II to prevent an excessive heat flux before the injection point of the film cooling, and a linear interpolation between regions II and III.

The optimized results for the cooling system can be observed in Fig. 7. As foreseen previously, the CHF could not overcome the heat flux in the whole engine contour. However, it was possible to fulfill this requirement for region I and region III. Consequently, the inclusion of film cooling is proposed to reduce the heat flux in the throat and be able to maintain a stable liquid-vapor interface. As well, the maximum wall temperature is respected. In terms of the coolant heat transfer coefficient, the existence of nucleate boiling at the start of coolant injection can be observed. This is evidenced by the coolant wall temperature exceeding the fluid's saturation temperature. As a result, nucleate boiling contributes significantly to the heat transfer coefficient considering that the coolant is in a subcooled state. The final pressure drop is around 4 bar. The importance of pressure drop lies on its relation with saturation temperature and the final coolant pressure which arrives at the injector. Finally the saturation margin is 18.84 K, which is undesirable low. Nevertheless, in order to be able to have a higher CHF it is necessary to have higher coolant velocities which, at the same time, increase the pressure drop, and thus, decrease the saturation margin. However, the further implementation of film cooling will ameliorate the final saturation margin.

4.2 Addition of film cooling

The injection of film cooling is intended to reduce the heat flux to prevent it from surpassing the critical heat flux (CHF). New variables are added to the design, the injection point and film mass flow. To determine these variables a sensibility study will be carried out taking into account the CHF, the maximum wall temperature, and the saturation margin. The injection point is to be ahead of the throat in order to decrease the maximum heat flux and temperature. The film mass flow will vary between 5% and 11% of the total coolant mass flow rate as shown in Tab. 2. Case 5 represents the best option in terms of maximum wall temperature, CHF and ΔT_{sub}.
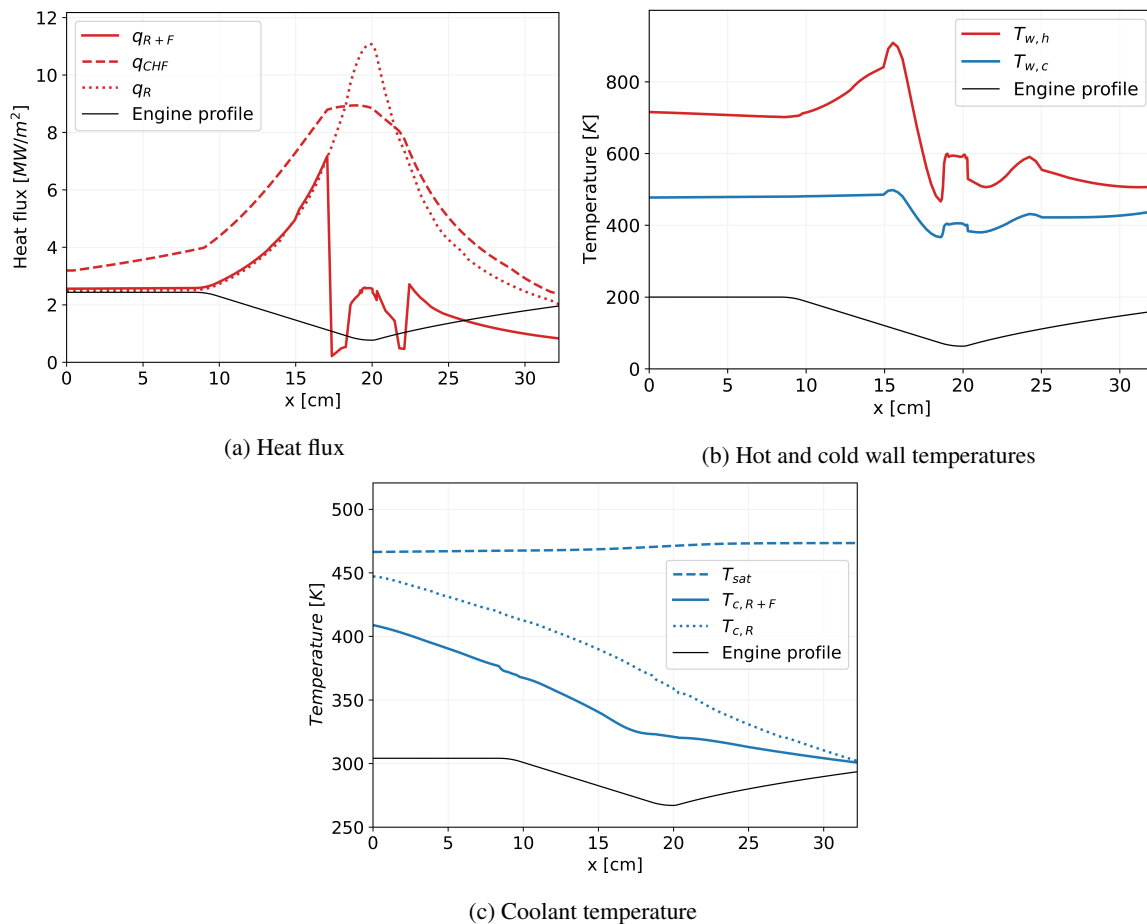

(a) Heat flux

(b) Hot and cold wall temperatures

(c) Coolant temperature

Figure 8: Results obtained with regenerative(R) + film cooling(R+F) along the engine axis

REGENERATIVE COOLING LIQUID ROCKET LOX/ETHANOL

Table 2: Film cooling sensibility study

	film mass flow	point of injection (m)	CHF > Heat flux	T_{max} (K)	ΔT_{sub} (K)
without film	-	-	No	1124.54	28.99
case 1	5%	0.1635	No	897.84	58.63
case 2	7%	0.136	No	1045.29	52.09
case 3	11%	0.140	Yes	1004.60	56.47
case 4	7%	0.140	Yes	1004.62	54.32
case 5	**7%**	**0.50**	**Yes**	**948.14**	**58.09**

The most significant change occurs at the injection point where the heat flux drops abruptly due to the presence of liquid film cooling. Fig. 8a illustrates the three different heat transfer mechanisms. Firstly the liquid film heats up and absorbed great part of the total heat flux. Downwards, the smooth rise of the heat flux is provoked by the throat proximity and the vaporization of the saturated liquid film which has a less effective heat transfer. Once, the liquid film has vaporized there is another discontinuity manifesting the change of state. Furthermore, the introduction of film cooling has enabled the CHF be greater than the heat flux in every region. As well, the saturation margin has decreased as a consequence of liquid film energy absorption. In the regenerative cooling system a saturation margin of 18.84 K is reached whereas the film cooling addition provokes a descent being the margin widened to 57.54 K. Finally, despite the injection of film cooling, the pressure drop reaches a value of 3.8 bar, since the velocity profile shows the same trend as for only regenerative cooling but with lower values.

5. Conclusion

A tool has been developed for the analysis of regenerative cooling systems in rocket engines. Due to the absence of specific experimental data for the LOX/Ethanol engine under investigation, the developed model was validated using CFD results obtained from a LOX/Methane engine experiment conducted by the Italian Aerospace Research Center (CIRA). Despite certain discrepancies between the model and CFD results, the comparison indicates that the one-dimensional model has the ability to produce preliminary analysis results that hold practical value.

Moreover, the study emphasizes the difficulties in accurately correlating heat transfer and boiling phenomena in rocket engines under extreme conditions. Existing models like Chen's and Gungor-Winterton's have limitations in predicting heat transfer at high heat flux levels. More experimental data is required to enhance and validate these correlations.

In the paper, the multi-objective optimization of the cooling system is discussed through the application of a genetic algorithm. The main objective of this optimization process is to determine the optimal geometry of the channels throughout the engine while considering important factors like maximum wall temperature, coolant saturation margin, and critical heat flux. The outcomes of the optimization yield a range of trade-off solutions, represented by a Pareto front, enabling the exploration of various compromises between the specified objectives. Furthermore, a film cooling model has been introduced as a solution to address the issue of disregarding the critical heat flux limitation across the entire engine system.

Overall, while the model may have limitations and uncertainties, the tool presented in this paper serves as a valuable resource for analyzing regenerative cooling systems in rocket engines. The optimization results provide insights into the design space and help identify suitable geometries for the cooling channels. Further research and experimental validation are necessary to refine the model and improve its accuracy.

6. Acknowledgments

References

[1] Liquid rocket engine self-cooled combustion chambers. Special Publication NASA-SP-8124, National Aeronautics and Space Administration, September 1977. Accession Number: 78N21211.

[2] D. R. Bartz. Turbulent Boundary-Layer Heat Transfer from Rapidly Accelerating Flow of Rocket Combustion Gases and of Heated Air. *Advances in Heat Transfer*, 1965.

[3] Ian H. Bell, Jorrit Wronski, Sylvain Quoilin, and Vincent Lemort. Pure and pseudo-pure fluid thermophysical property evaluation and the open-source thermophysical property library coolprop. *Industrial & Engineering Chemistry Research*, 53(6):2498–2508, 2014.

[4] B. Betti, D. Liuzzi, F. Nasuti, and M. Onofri. Development of heat transfer correlations for lox/ch4 thrust chambers.

[5] G.P. Celata, M. Cumo, and A. Mariani. Assessment of correlations and models for the prediction of chf in water subcooled flow boiling. *International Journal of Heat and Mass Transfer*, 37(2):237–255, 1994.

[6] J. C. Chen. Correlation for boiling heat transfer to saturated fluids in convective flow. *Industrial & Engineering Chemistry Process Design and Development*, 5(3):322–329, 1966.

[7] Lin Chen, Pei Zhou, Ronghua Huang, Xi Han, Shiyang Hua, Zhi Li, and Lei Gao. Experimental investigation on the suppression factor in subcooled boiling flow. *Applied Thermal Engineering*, 135:549–558, 2018.

[8] Weiwei Chen and Xiande Fang. A note on the chen correlation of saturated flow boiling heat transfer. *International Journal of Refrigeration*, 48:100–104, 2014.

[9] M. G. Cooper. Saturation nucleate pool boiling - a simple correlation. pages 785–793, 1984.

[10] K. Deb, A. Pratap, S. Agarwal, and T. Meyarivan. A fast and elitist multiobjective genetic algorithm: Nsga-ii. *IEEE Transactions on Evolutionary Computation*, 6(2):182–197, 2002.

[11] H. K. Forster and N. Zuber. Dynamics of vapor bubbles and boiling heat transfer. *AIChE Journal*, 1(4):531–535, 1955.

[12] William M. Grisson. Liquid film cooling in rocket engines. Technical report, United States Air Force, 1991.

[13] K.E. Gungor and R.H.S. Winterton. A general correlation for flow boiling in tubes and annuli. *International Journal of Heat and Mass Transfer*, 29(3):351–358, 1986.

[14] Wen-Tao Ji, Chuang-Yao Zhao, Ya-Ling He, and Wen-Quan Tao. Experimental validation of cooper correlation at higher heat flux. *International Journal of Heat and Mass Transfer*, 90:1241–1243, 2015.

[15] S. G. Kandlikar. Heat Transfer Characteristics in Partial Boiling, Fully Developed Boiling, and Significant Void Flow Regions of Subcooled Flow Boiling. *Journal of Heat Transfer*, 120(2):395–401, 05 1998.

[16] C. U. Kirchberger. Investigation on heat transfer in small hydrocarbon rocket combustion chambers. 2014.

[17] B. M. Lekakh, M. S. Kazimi, and J. E. Meyer. Boiling heat transfer for high velocity flow of highly subcooled water. Technical Report MITNE-315, Massachusetts Institute of Technology, October 1998.

[18] Marco Leonardi, Marco Pizzarelli, and Francesco Nasuti. Analysis of thermal stratification impact on the design of cooling channels for liquid rocket engines. *International Journal of Heat and Mass Transfer*, 135:811–821, 2019.

[19] R. Mastrullo, A.W. Mauro, R. Revellin, and L. Viscito. Flow boiling heat transfer and pressure drop of pure ethanol (99.8%) in a horizontal stainless steel tube at low reduced pressures. *Applied Thermal Engineering*, 145:251–263, 2018.

[20] Marco Pizzarelli, Barbara Betti, Francesco Nasuti, Daniele Ricci, Pietro Roncioni, Francesco Battista, and Vito Salvatore. Cooling channel analysis of a lox/lch4 rocket engine demonstrator.

[21] M Popp and G Schmidt. Rocket engine combustion chamber design concepts for enhanced life, 1996.

[22] Annafederica Urbano and Francesco Nasuti. Parametric analysis of heat transfer to supercritical-pressure methane. *Journal of Thermophysics and Heat Transfer*, 27(4):674–685, 2013.